

GAS SHEPHERDING BY AN INFALLING SATELLITE

PHILIP CHANG^{1,2}

Draft version November 17, 2018

ABSTRACT

I calculate the action of a satellite, infalling through dynamical friction, on a coplanar gaseous disk of finite radial extent. The disk tides, raised by the infalling satellite, couple the satellite and disk. Dynamical friction acting on the satellite then shrinks the radius of the coupled satellite-disk system. Thus, the gas is “shepherded” to smaller radii. In addition, gas shepherding produces a large surface density enhancement at the disk edge. If the disk edge then becomes gravitationally unstable and fragments, it may give rise to enhanced star formation. On the other hand, if the satellite is sufficiently massive and dense, the gas may be transported from ~ 100 pc to inside of a 10 to 10s of parsecs before completely fragmenting into stars. I argue that gas shepherding may drive the fueling of active galaxies and central starbursts and I compare this scenario to competing scenarios. I argue that sufficiently large and dense super star clusters (acting as the shepherding satellites) can shepherd a gas disk down to ten to tens of parsecs. Inside of ten to tens of parsecs, another mechanism may operate, i.e., cloud-cloud collisions or a marginally (gravitationally) stable disk, that drives the gas $\lesssim 1$ pc, where it can be viscously accreted, feeding a central engine.

Subject headings: galaxies: nuclei – galaxies: starburst – galaxies: star clusters – accretion, accretion disks

1. INTRODUCTION

The tidal interaction between small satellites and the gas or particle disks in which they are embedded is a subject of wide study in the planetary community. These satellites are tidally coupled via disk tides, i.e., satellites excite spiral density waves at the Lindblad resonances in the disk (Goldreich & Tremaine 1978, 1980; Artymowicz 1993). As a result of these tidal interactions, gaps can be opened up in the embedded disks as in the case of the shepherding moons of Saturn’s rings (Goldreich & Tremaine 1978) or in type-II migration (Ward 1997). Alternatively, if a gap does not open up, satellite may migrate inward rapidly due to tidal torque imbalances, i.e., type-I migration (Ward 1997).

The wide applicability of satellite-disk interactions in the planetary community raises an interesting question of whether the same physics may be applicable at larger scales, i.e., galactic scales. In this paper, I will address this question by considering a very simple model, which illustrate the modification of the physics of satellite-disk interaction when applied on a galactic scale. Most notably, the critical difference is that in addition to tidal torques, the satellite will experience dynamical friction. The inclusion of dynamical friction produces a non-trivial effect. Namely, dynamical friction on the satellite provides a sink of angular momentum in the system. As a result, the coupled satellite-disk system will continually lose angular momentum and sink toward the center.

To study this physics, I consider a very simple model. In my model, a satellite starts out in a circular orbit at a large radius and sinks toward the central mass concentration because of dynamical friction on the background stars. Along its infall, it encounters a coplanar gaseous

disk or ring, which initially has a finite radial extent, $r_{d,0}$. Tides begin to couple the satellite with the disk. Because the satellite-disk system continues to suffer an ongoing loss of angular momentum from dynamical friction, it will shrink in radius. As a result gas can be transported on the dynamical friction timescale to smaller radii. In addition, I find that this satellite-disk interaction also builds a substantial surface density enhancement at the disk edge. This may lead to enhanced star formation at the disk edge. This process which I call *gas shepherding* may be a generic feature of gaseous disks around galaxies, if a sufficiently massive and dense satellite is available.

The physics of satellite-disk interactions in galaxies or gas shepherding is not just an interesting exercise in mathematical physics, but may be important in the fueling of active galaxies and central starbursts. First, the action of dynamical friction on the satellite-disk system will shrink radius of the disk, thereby transporting gas to smaller radii. This shepherding of gas will continue until the gas is forced into the center or the shepherding satellite is destroyed. I will discuss this scenario for nuclear fueling and how it compares to competing scenarios in this paper.

I have structured this paper as follows. In §2, I discuss the basic picture of gas shepherding and give a few order of magnitude estimates. I estimate the timescale for gas shepherding and the expected surface density enhancement. I present the physics of gas shepherding and solve numerical models in §3. I also present an approximate analytic solution to this problem. I then discuss the application of gas shepherding to the feeding of active galactic nuclei and central starbursts in §4. Finally I present my conclusions in §5.

2. BASIC PICTURE

The basic picture of gas shepherding is illustrated by Figure 1. A gas disk with a radius of r_d and surface density of Σ orbits about a spherical mass distribution

¹ Astronomy Department and Theoretical Astrophysics Center, 601 Campbell Hall, University of California, Berkeley, CA 94720; pchang@astro.berkeley.edu

² Miller Institute for Basic Research

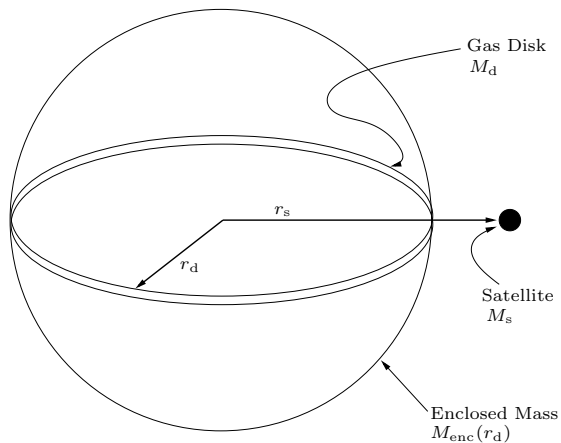


FIG. 1.— Schematic of gas shepherding. A satellite with mass, M_s , and orbital radius, r_s , infalls via dynamical friction and interacts with a gaseous disk with mass, $M_d = \pi\Sigma r_d^2$, that sits in a halo with total enclosed mass, M_{enc} .

with enclosed mass of stars or dark matter of $M_{\text{enc}}(r_d)$. Due to dynamical friction on the stellar background, an external satellite with mass M_s slowly spirals in on a circular orbit with a radius of r_s in the same orbital plane of the gas disk. The radial velocity at which the satellite initially spirals into the gas disk due to dynamical friction is $v_{\text{df}} \sim (M_s/M_{\text{enc}})v_{\text{orb}}$, where v_{orb} is the orbital velocity of the satellite. As the satellite approaches the disk edge, i.e., r_s approaches r_d , the satellite excites spiral density waves at the Lindblad resonances (Goldreich & Tremaine 1980), which transfers angular momentum from the disk to the satellite. This angular momentum is in turn transferred to the background stars or dark matter via dynamical friction on the satellite. Since angular momentum of the satellite-disk system is continually bled, the radius of the satellite-disk system will shrink at the shepherding velocity, v_{shep} .

I first give some simple order of magnitude estimates of this process. The dynamical friction timescale for a satellite is (Chandrasekhar 1943; Binney & Tremaine 1987)

$$t_{\text{df}} \sim \frac{M_{\text{enc}}}{M_s} t_{\text{dyn}}, \quad (1)$$

where $t_{\text{dyn}} = \Omega_s^{-1}$ is the dynamical time, $\Omega_s = \sqrt{GM_{\text{enc}}/r_s^3}$ is the orbital frequency of the satellite, and G is Newton's constant. The torque due to dynamical friction on the satellite, T_{df} , is

$$T_{\text{df}} \sim M_s r_s^2 \Omega_s t_{\text{df}}^{-1} \sim \frac{GM_s^2}{r_s} \quad (2)$$

The torque due to the excitation of spiral density waves in a disk is (Goldreich & Tremaine 1980; Lin & Papaloizou 1986; Ward & Hourigan 1989; Artymowicz 1993; Ward 1997)

$$T_d \sim \frac{GM_s^2}{r_s} \frac{M_d}{M_{\text{enc}}} \left(\frac{r_s}{r_s - r_d} \right)^3, \quad (3)$$

where $M_d = \pi\Sigma r_d^2$ is the mass of the disk, I have presumed that radial separation between satellite and disk is small compared to the radius, i.e., $r_s - r_d \ll r_s$.

For now, I assume that there is no internal rearrangement of angular momentum in the disk, i.e., an inviscid

disk. Dynamical friction torques down the satellite (T_{df}), while the disk, whose edge sits at $r_d < r_s$, torques up the satellite (T_d). When $T_{\text{df}} \sim T_d$, the satellite and the disk are well coupled for $M_s \leq M_d$, i.e., the mass of the satellite is smaller or comparable to the mass of the disk. Setting $T_{\text{df}} \sim T_d$ gives

$$\frac{r_s - r_d}{r_s} \sim \left(\frac{M_d}{M_{\text{enc}}} \right)^{1/3}, \quad (4)$$

which I define as the ‘‘Hill’’ radius of the disk, $r_{\text{H,d}} = r_s (M_d/M_{\text{enc}})^{1/3}$.³ This gives the natural scale for the radial separation between disk and satellite, i.e., $r_s - r_d \sim r_{\text{H,d}}$.

For spiral density waves that damp locally, the radial extent of the disk over which the satellite exerts torques is also $\sim r_{\text{H,d}}$. Assuming no viscous spreading, the disk surface density will be enhanced at the disk edge due to the piling up of material from the initial radius of $r_{d,0}$ to the current radius of r_d . This enhancement due to a satellite that sinks a distance $\sim r_d$ is

$$\frac{\Sigma}{\Sigma_0} \sim r_d/r_{\text{H,d}}, \quad (5)$$

where Σ is the surface density and Σ_0 is the initial surface density. For $M_d/M_{\text{enc}} \sim 10^{-3} - 10^{-2}$, the enhancement is a factor of a few to ten.

3. GAS SHEPHERDING

3.1. Basic Equations

To study this problem in greater detail, I begin by writing the equations for a viscous disk that is evolving under the influence of an external torque. The equation of continuity is

$$\frac{\partial \Sigma}{\partial t} + \frac{1}{r} \frac{\partial (r \Sigma v_r)}{\partial r} = 0, \quad (6)$$

where r is the radial coordinate, and v_r is the radial component of the velocity (Frank, King, and Raine 2002). The angular momentum equation is

$$\Sigma \frac{\partial (r^2 \Omega)}{\partial t} + v_r \Sigma \frac{\partial (r^2 \Omega)}{\partial r} = -\frac{1}{2\pi r} \left(\frac{\partial T_{\text{visc}}}{\partial r} - \frac{\partial T_d}{\partial r} \right), \quad (7)$$

where $\Omega = \sqrt{GM_{\text{enc}}(r)/r^3}$ is the orbital frequency, $M_{\text{enc}}(r)$ is the mass enclosed inside r , and $T_{\text{visc}} = -2\pi r^3 \nu \Sigma \partial \Omega / \partial r$ is the viscous torque, ν is the viscosity (Frank, King, and Raine 2002). Using equation (7), I find⁴

$$v_r = -\frac{1}{2\pi r \Sigma} \left(\frac{\partial (r^2 \Omega)}{\partial r} \right)^{-1} \left[\frac{\partial}{\partial r} (T_{\text{visc}} - T_d) \right]. \quad (8)$$

Plugging equation (8) into (6), I find

$$\frac{\partial \Sigma}{\partial t} = \frac{1}{2\pi r} \frac{\partial}{\partial r} \left(\frac{\partial (r^2 \Omega)}{\partial r} \right)^{-1} \left[\frac{\partial}{\partial r} (T_{\text{visc}} - T_d) \right]. \quad (9)$$

³ I use quotation marks because disks do not have Hill radii in the traditional sense. Rather I have adopted this terminology because of the familiar scaling, i.e., the 1/3 power law.

⁴ The angular frequency, Ω is a function only of the coordinate, r , assuming that the mass enclosed, i.e., M_{enc} is not an explicit function of time. Therefore, the first term completely disappears from equation (7).

For the torque density due to an orbiting satellite on a disk, $\partial T_d/\partial r$, I take a form suggested by Ward & Hourigan (1989) (see also Goldreich & Tremaine 1980; Lin & Papaloizou 1979a, 1979b, 1986):

$$\frac{\partial T_d}{\partial r} = \text{sgn}(r - r_s) \beta \frac{G^2 M_s^2 \Sigma}{r(\Omega - \Omega_s)^2 (r - r_s)^2}, \quad (10)$$

where β is a constant of order unity. For $|r - r_s| \ll r$, I expand $\Omega - \Omega_s \approx (\partial\Omega/\partial r)(r - r_s)$ to get

$$\frac{\partial T_d}{\partial r} \approx \text{sgn}(r - r_s) \beta \frac{G^2 M_s^2 \Sigma r}{\Omega^2 (r - r_s)^4}, \quad (11)$$

where I have taken a density profile for the enclosed mass of the form $\rho \propto r^{-2}$, so that

$$M_{\text{enc}}(r) = M_{\text{enc},0} \frac{r}{r_0}, \quad (12)$$

where $M_{\text{enc},0}$ is the enclosed mass at r_0 . Note that for such a mass distribution, the orbital velocity, $v_{\text{orb}} = \sqrt{GM_{\text{enc},0}/r_0}$, is a constant. Using (12), I find the following relations

$$\frac{\partial T_{\text{visc}}}{\partial r} = 2\pi v_{\text{orb}} \frac{\partial}{\partial r} (\Sigma \nu r), \quad (13)$$

$$\frac{\partial T_d}{\partial r} \approx \text{sgn}(r - r_s) \beta \frac{GM_s^2 \Sigma r_0 r^3}{M_{\text{enc},0} (r - r_s)^4}, \quad (14)$$

Plugging equations (13) and (14) into (9), I find

$$\frac{\partial \Sigma}{\partial t} = \frac{1}{r} \frac{\partial^2 (r\nu\Sigma)}{\partial r^2} + \frac{\beta}{2\pi} \frac{r_0}{v_{\text{orb}} r} \frac{GM_s^2}{M_{\text{enc},0}} \frac{\partial}{\partial r} \left[\frac{\Sigma r^3}{(r - r_s)^4} \right], \quad (15)$$

where I assume $r < r_s$, which fixes the sign. Note that the term in equation (8) and (9), $\partial(r^2\Omega)/\partial r = v_{\text{orb}}$, is a constant using the prescribed mass distribution in equation (12). I chose the viscosity law suggested by Lin & Papaloizou (1986):

$$\nu = \nu_0 \left(\frac{\Sigma}{\Sigma_0} \right)^2. \quad (16)$$

The time-rate change of angular momentum of the satellite is

$$M_s \frac{\partial(r_s^2 \Omega_s)}{\partial t} = -T_d + T_{\text{df}}, \quad (17)$$

where $-T_d = -\int dr \partial T_d/\partial r$. The velocity of infall, i.e., the shepherding velocity, is $v_{\text{shep}} = \dot{r}_s$. Thus, I find

$$\frac{\partial r_s}{\partial t} = \frac{GM_s}{v_{\text{orb}}} \left[-\beta \int \frac{\text{sgn}(r - r_s) \Sigma r_0 r^3}{(r - r_s)^4 M_{\text{enc},0}} dr - \ln \Lambda \frac{1}{r_s} \right] \quad (18)$$

Equations (15) and (18) constitute a complete set of equations which governs the behavior of the satellite-disk system. These equations are exactly the same as those that govern the migration of protoplanets in protoplanetary nebula (Lin & Papaloizou 1979ab, 1986; Hourigan & Ward 1984; Ward & Hourigan 1989; Ward 97; Rafikov 2002), except with the addition of another term on the RHS of equation (18), which is due to dynamical friction.

To simplify equations (15) and (18), I rescale the variables

$$\sigma = \frac{\Sigma}{\Sigma_0}, \quad (19)$$

$$t' = \frac{t}{t_{\text{df}}} = \Omega_0 t \ln \Lambda \frac{M_s}{M_{\text{enc},0}}, \quad (20)$$

where Σ_0 is the initial surface density of the disk, which I assume to be constant and Ω_0 is the orbital frequency at $r = r_0$. Equations (15) and (18) become

$$\frac{\partial \sigma}{\partial t'} = \frac{\nu_0}{q\Omega_0 \ln \Lambda r} \frac{\partial^2 (r\sigma^3)}{\partial r^2} + \beta' \frac{qr_0^3}{r} \frac{\partial}{\partial r} \left(\frac{\sigma r^3}{(r - r_s)^4} \right) \quad (21)$$

$$\frac{\partial r_s}{\partial t'} = 2\beta' \frac{\pi \Sigma_0 r_0^2}{M_{\text{enc},0}} r_0 \int \frac{\sigma r^3}{(r - r_s)^4} dr - \frac{r_0^2}{r_s} \quad (22)$$

where $q = M_s/M_{\text{enc},0}$ and $\beta' = \beta/(2\pi \ln \Lambda)$, and I have taken the viscosity to be $\nu = \nu_0 \sigma^2$ (see eq.[16]), where $\nu_0 = \alpha(h_{\text{d},0}/r_{\text{d},0})^2 r_{\text{d},0} v_{\text{orb}}$,⁵ where $r_{\text{d},0}$ is the initial radius, $h_{\text{d},0}$ is the initial vertical scale height of the disk, and α dimensionless viscosity parameter (Frank, King, & Raine 2002). The initial scale height of the disk can be written as $h_{\text{d},0}/r_{\text{d},0} = Q_0 q_{\text{d}}/\sqrt{2}$,⁶ where Q_0 is the initial Toomre Q (Toomre 1964) of the disk and $q_{\text{d}} = M_{\text{d}}/M_{\text{enc},0}$ is the ratio of the disk mass to the enclosed mass. Without loss of generality, I now take $r_0 = r_{\text{d},0} \approx r_{\text{s},0}$ to find

$$\frac{\partial \sigma}{\partial t'} = \alpha' \frac{q_{\text{d}}}{q'} \frac{r_{\text{d},0}^2}{r} \frac{\partial^2 (r\sigma^3)}{\partial r^2} + \beta' \frac{q' q_{\text{d}} r_{\text{d},0}^3}{r} \frac{\partial}{\partial r} \left(\frac{\sigma r^3}{(r - r_s)^4} \right), \quad (23)$$

$$\frac{\partial r_s}{\partial t'} = 2\beta' q_{\text{d}} r_{\text{d},0} \int \frac{\sigma r^3}{(r - r_s)^4} dr - \frac{r_{\text{d},0}^2}{r_s} \quad (24)$$

where $q' = M_s/M_{\text{d}}$ and $\alpha' = \alpha Q_0^2/(2 \ln \Lambda)$. Equations (23) and (24) are the master equations governing my model which I solve numerically in §3.2 and solve approximately in §3.3.

3.2. Numerical Results

Equations (23) and (24) consists of four dimensionless parameters: q_{d} , q' , α' and β' . For the dimensionless parameters, β' , which represent the relative power between disk tides and dynamical friction, I choose a fiducial value for $\beta' = 1$, assuming fiducial values of $\ln \Lambda \sim O(1)$ and $\beta \sim O(1)$. For α' , which represents the relative power between viscosity and dynamical friction, I take $\alpha' = 10^{-3} - 10^{-1}$ to study the effects of viscosity. Finally, I set $q_{\text{d}} = M_{\text{d}}/M_{\text{enc}} = 10^{-3}$.

I solve equations (23) and (24) using standard explicit finite-difference methods (Press et al. 1992). For good spatial resolution, I select 750 grid points between

⁵ Using the standard Shakura & Sunyaev (1973) α prescription for the viscosity, i.e. $\nu = \alpha c_s h$, where c_s is the sound speed and h is the disk scale height, I write $c_s = v_{\text{orb}} h/r$ and I take $h = h_{\text{d},0}$ at $r = r_{\text{d},0}$.

⁶ To get this relation, take the Toomre Q parameter for a gaseous disk, $Q = c_s \kappa_0 / \pi G \Sigma_0$ (Binney & Tremaine 1987). The epicyclic frequency, $\kappa_0 = (4 + 2d \ln \Omega_0 / d \ln r)^{1/2} \Omega_0 = \sqrt{2} \Omega_0$. Plugging $c_s = v_{\text{orb}} h/r$, I find $h/r = (M_{\text{d}}/M_{\text{enc}})(Q/\sqrt{2})$.

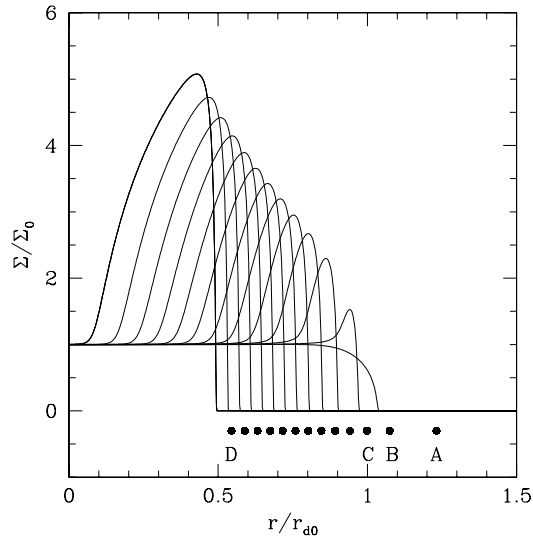


FIG. 2.— Evolution of the surface density as a function of radius for a satellite disk system where $q' = 0.1$ for $\alpha' = 0.1$ and $\beta' = 1$. The snapshots are separated in $\Delta t = 0.25t_{\text{df},0}$ increments. The satellite position is marked by the black dot below the surface density plot. Each point and each curve correspond to one snapshot. The labeled points, A-D, are explained in the text.

$r/r_{d,0} = 0$ to 1.5 with the satellite initially at $r_s = 2r_{d,0}$. The satellite begins to fall inward via dynamical friction. As the satellite approaches the disk, the disk exerts a torque on the satellite, which slows its infall. At the same time, the surface density of the disk increases at the disk edge.

I show this evolution for $\alpha' = 0.1$, $\beta' = 1$, and $q' = 0.1$ in Figure 2. I start the evolution of the satellite at $r_s/r_{d,0} = 2$. When the satellite sinks to $r_s/r_{d,0} = 1.25$, I set $t = 0$ and plot the evolution of the satellite-disk system in intervals of $\Delta t = 0.25t_{\text{df},0}$ for a total of $1.75t_{\text{df},0}$ where $t_{\text{df},0}$ is the dynamical friction timescale at $r_{d,0}$. At $t = 0$ the disk is undisturbed except for a small amount of spreading due to viscosity at the disk edge. The satellite position is at $r/r_{d,0} \approx 1.25$ as noted by the black dot labeled A. I evolve in intervals of Δt and note that the disk satellite system has begun to respond (point labeled B). The disk begins to develop a surface density enhancement and the satellite slows down a bit. Evolving for another Δt , i.e., the point labeled C, shows a substantial change. The surface density increases near the disk edge by a maximum factor of ≈ 2 . Note that the distance between point B and C is substantially smaller than the distance between A and B, which results from the backreaction of the disk tides. By point D, the density enhancement is ≈ 5 . Note also that the distance between point D and its neighbor is somewhat larger than the other separations. This is due to the decrease in the dynamical friction timescale compared to the dynamical timescale when the mass enclosed decreases relative to the satellite mass.

In Figure 3 and 4, I show the case for $q' = 0.01$ and 1 respectively. For $q' = 0.01$ (Fig. 3), the initial infall of the satellite is stopped by the disk because of the large mass ratio between the satellite and the disk. In addition, there is no surface density enhancement at the disk edge. For $q' = 1$ (Fig. 4), on the other hand, the initial infall of the satellite is only slightly slowed because the mass of

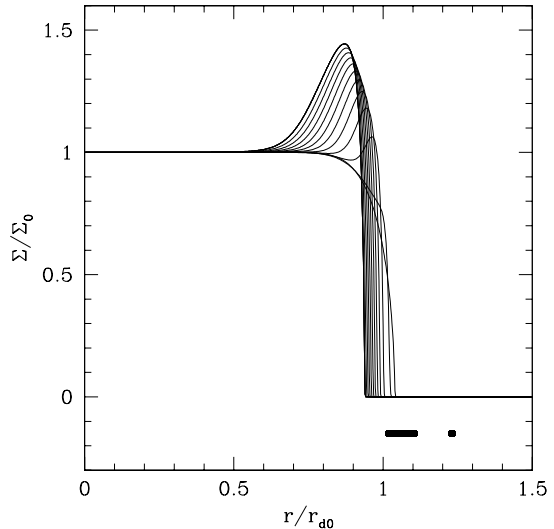


FIG. 3.— Same as Figure 2 but for $q' = 0.01$. The larger mass of the disk stops the body from infalling toward the center. In this case there is no surface density enhancement.

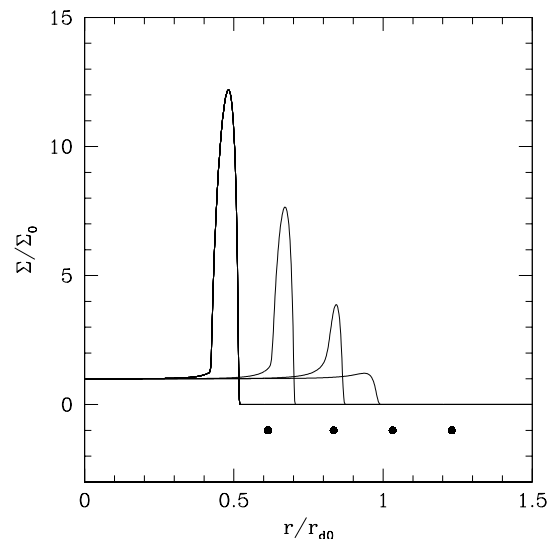


FIG. 4.— Same as Figure 2 but for $q' = 1$. The surface density is enhanced over the case where $q' = 0.1$. In addition the disk has a much reduced effect on the infall velocity of the satellite because they have equal masses.

the disk and satellite are the same. In this case, a huge surface density enhancement is produced.

One remarkable aspect of Figures 2 and 4 is that they appear to approach quasi-steady state solutions. This is especially clear in Figure 2. Motivated by the appearance of these quasi-steady state solutions, I find an approximate kinematic wave solution in §3.3, which agrees well with these numerical results.

In Figure 5, I plot the normalized shepherding velocity of the satellite disk system, i.e., normalized to the initial infall velocity, $v_{\text{df},0} = v_{\text{df}}(r_{d,0})$ (lower plot) and the local infall velocity, v_{df} (upper plot), as a function of r_s for $q' = 0.01, 0.1$, and 1. I plot it for $\alpha' = 0.001, 0.01$, and 0.1. For comparison I plot the local dynamical friction infall velocity, $v_{\text{df}}(r_s)$. For $r_s > r_{d,0}$, $v_{\text{shep}} \approx v_{\text{df}}$ because tidal coupling between the disk and satellite has not yet

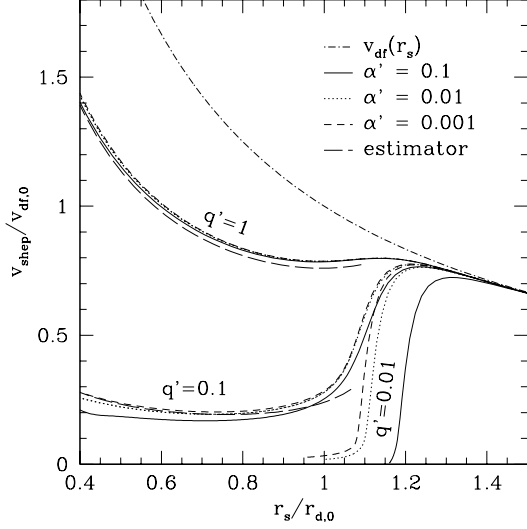


FIG. 5.— Plot of the normalized shepherding velocity as a function of r_s for $q' = 0.01$ (bottom set of curves), 0.1 (middle set), and 1 (top set) and $\alpha' = 0.001$ (short-dashed lines), 0.01 (dotted lines), and 0.1 (solid lines) normalized to the initial infall velocity, $v_{df,0}$. The local dynamical infall velocity, v_{df} (dot-dashed line), is also plotted for purposes of comparison. Finally, the estimate for v_{shep} (eq.[41]) is plotted for $r_s < r_{d,0} - r_{H,d}$ to allow a kinematic wave solution to be established.

been achieved. Once the coupling has been achieved, i.e. $r_s < r_{d,0}$, the shepherding velocity depends mainly on the mass ratio between the satellite and disk, q' , and is independent of the viscosity, α' . This highlights the fact that dynamical friction dominates the dynamics. I also plot an estimate for migration velocity (eq.[41]) for $r_s < r_{d,0} - r_{H,d}$, i.e., I allow the shepherding satellite to fall inside of one Hill radius of the disk to allow a kinematic wave solution to be set up (see §3.3). This estimate (eq.[41]) gives remarkably good results, i.e., $\lesssim 10\%$ for the fiducial cases of $q' = 0.1$ and 1. The most remarkable aspect of Figure 5 is that while the infall velocity falls substantially, a sizeable fraction of the initial infall velocity remains. For instance, the infall velocity does not fall below 20% of the initial infall velocity for the $q' = 0.1$ case.

The shepherding satellite transports gas from large radii to smaller radii by dumping the angular momentum of the gas into the background stars or dark matter. Moreover, this transport is achieved on a dynamical friction timescale, which can be fast for sufficiently massive satellites. This transport will continue unless the gas is consumed via star formation or the satellite is tidally disrupted by the increasing density of the background (see §4.3).

3.3. Approximate Solution

Motivated by the numerical results of §3.2 I now solve equations (23) and (24) using a kinematic wave approach inspired by the planetary literature (Hourigan & Ward 1984; Ward & Hourigan 1989; Ward 1997; Rafikov 2002). First I approximate equations (23) and (24) to recover a simpler set. As the order of magnitude estimate in §2 reveals, the typical radial separation for a well coupled satellite-disk system is the Hill radius of the disk, $r_{H,d}$. Thus, I now change variables in equations (23) and (24)

from r to x , where

$$x = \frac{r - r_s}{r_{H,d,0}} = \frac{r - r_s}{q_d^{1/3} r_{d,0}}, \quad (25)$$

where $r_{H,d,0} = q_d^{1/3} r_{d,0}$ is the *initial* Hill radius of the disk. Since $r_{H,d,0} \ll r$, I take the approximation $r - r_s \ll r$ to find

$$\frac{\partial \sigma}{\partial t'} = \alpha' \frac{q_d^{1/3}}{q'} \frac{\partial^2 \sigma^3}{\partial x^2} + \frac{q'}{q_d^{2/3}} \beta' \left(\frac{x_s}{x_{d,0}} \right)^2 \frac{\partial}{\partial x} \left(\frac{\sigma}{x^4} \right), \quad (26)$$

$$\frac{\partial x_s}{\partial t'} = x_{d,0} \left[2\beta' \left(\frac{x_s}{x_{d,0}} \right)^3 \int \frac{\sigma}{x^4} dx - \frac{x_{d,0}}{x_s} \right], \quad (27)$$

where $x_s = r_s/r_{H,d}$ and $x_{d,0} = r_{d,0}/r_{H,d}$.⁷

I now assume the kinematic wave *ansatz*: $\sigma = \sigma_w(x - v_{shep}t')$, where σ_w denotes my kinematic wave solution for σ . Inserting this *ansatz* into equation (26), I find:

$$-v_{shep} \frac{\partial \sigma_w}{\partial x} = \alpha' \frac{q_d^{1/3}}{q'} \frac{\partial^2 \sigma_w^3}{\partial x^2} + \frac{q'}{q_d^{2/3}} \beta' \left(\frac{x_s}{x_{d,0}} \right)^2 \frac{\partial}{\partial x} \frac{\sigma_w}{x^4}, \quad (28)$$

Integrating once and ignoring the constant of integration, I find

$$-v_{shep} = \frac{3\alpha' q_d^{1/3}}{2 q'} \frac{\partial \sigma_w^2}{\partial x} + \frac{q'}{q_d^{2/3}} \beta' \left(\frac{x_s}{x_{d,0}} \right)^2 \frac{1}{x^4}, \quad (29)$$

where I have cancelled one factor of σ_w from each term. I now integrate once more to find

$$\sigma_w^2 = C + \frac{q'}{\alpha' q_d^{1/3}} \left(-\frac{2}{3} v_{shep} x + \frac{2\beta'}{9} \left(\frac{x_s}{x_{d,0}} \right)^2 \frac{q'}{q_d^{2/3}} \left(\frac{1}{x^3} \right) \right), \quad (30)$$

where C is the constant of integration. The two terms in the parenthesis are both negative because $x \propto r - r_s < 0$ and $v_{shep} < 0$ (inward migration). The first term in the parenthesis cuts off the surface density as x becomes more negative, i.e., away from the disk edge, while the second term cuts off the surface density as it approaches the disk edge due to tidal interactions. The peak, i.e., where σ_w^2 is maximal, is found from equation (29) by setting $\partial \sigma_w^2 / \partial x = 0$. This occurs when⁸

$$x = x_{peak} \equiv - \left(\frac{q'}{q_d^{2/3}} \beta' \left(\frac{x_s}{x_{d,0}} \right)^2 \frac{1}{-v_{shep}} \right)^{1/4}. \quad (31)$$

Hence, $\sigma_w(x_{peak}) = \sigma_{max}$, so given an estimate for σ_{max} , I can determine the constant of integration, C , via

$$C = \sigma_{max}^2 - \frac{q'}{\alpha' q_d^{1/3}} \left(-\frac{2}{3} v_{shep} x_{peak} \right)$$

⁷ To aid in the derivation of equation (26) and (27), it is helpful to consider which terms will change rapidly for small x and which terms will change slowly. For instance, the term $(r - r_s)^{-4} \rightarrow x^{-4}$ changes rapidly with small x , whereas $r \rightarrow r = r_s + r_{H,d} x \approx r_s$ changes very slowly. Hence, I made the following series of substitutions $r \rightarrow r_s$ and $r - r_s \rightarrow r_{H,d} x$.

⁸ To clarify the signs in equation (31), note that $x < 0$, i.e., the satellite is at larger radii than the gas and $v_{shep} < 0$, i.e., the satellite-disk system moves inward.

$$+ \frac{2\beta'}{9} \left(\frac{x_s}{x_{d,0}} \right)^2 \frac{q'}{q_d^{2/3}} \left(\frac{1}{x_{\text{peak}}^3} \right), \quad (32)$$

In the appendix, I calculate σ_{max} by balancing the torque from the satellite-disk interaction with the torque from dynamical friction. I find the following cubic equation (eq.[A13]):

$$\frac{2\beta'}{3} \frac{\sigma_{\text{max}}}{x_{\text{peak}}^3} + 2 \left(\frac{x_{d,0}}{x_s} \right)^2 \frac{\alpha' q_d}{q'^2} \sigma_{\text{max}}^3 - \left(\frac{x_{d,0}}{x_s} \right)^4 = 0, \quad (33)$$

which I solve numerically. This gives an estimate for σ_{max} and hence, C , given v_{shep} . Therefore, to complete the calculation, I now give an estimate for v_{shep} . Before I do so, I note that the RHS of equation (30) can be negative. To join this kinematic wave solution, σ_w , onto the background solution, I set

$$\sigma^2 = \begin{cases} \sigma_w^2 & \text{if } \sigma_w^2 > 0 \text{ and } x > x_{\text{peak}} \\ \sigma_w^2 & \text{if } \sigma_w^2 > 1 \text{ and } x < x_{\text{peak}} \\ 0 & \text{if } \sigma_w^2 < 0 \text{ and } x > x_{\text{peak}} \\ 1 & \text{if } \sigma_w^2 < 1 \text{ and } x < x_{\text{peak}} \end{cases}. \quad (34)$$

I now proceed to calculate v_{shep} . I estimate the torque using equation (2). The satellite raises tides on the disk, which do not operate over the entire disk, i.e. the tides are most acute at the edge of the disk due to the $(r - r_s)^{-4}$ scaling of the torque density. Rather they act on the accumulated mass at the disk edge, M_{edge} , which I estimate to be:

$$M_{\text{edge}} \approx M_d \left[1 - \left(\frac{r_{d,\text{edge}}}{r_{d,0}} \right)^2 \right], \quad (35)$$

where $r_{d,\text{edge}}$ is the edge of the disk.⁹ To estimate $r_{d,\text{edge}}$ for equation (35), I presume the following fit

$$r_{d,\text{edge}} = r_s - \psi r_{\text{H},d,0}, \quad (36)$$

where ψ is a constant of order unity and is determined below. The total angular momentum of the satellite-disk system over which these torques are effective is

$$L = v_{\text{orb}} (M_s r_s + M_{\text{edge}} r_d). \quad (37)$$

The difference between r_d and r_s is of order the Hill radius of the disk, $r_{\text{H},d} = r_d (M_d/M_{\text{enc}})^{1/3}$ (see §2). As the satellite falls inward and builds a large surface density enhancement, I expect that the Hill radius of the disk will change, i.e., $\Sigma_0 \rightarrow \Sigma \approx M_{\text{edge}}/4\pi r_d r_{\text{H},d}$, where I assume that the mass of the edge is spread over a radial thickness of $r_{\text{H},d}$. Therefore, I define an effective Hill radius of the disk by

$$\frac{r_{\text{H},\text{eff}}}{r_d} = \left(\frac{\pi \Sigma(r_d) r_d^2}{M_{\text{enc}}} \right)^{1/3}, \quad (38)$$

$$= \frac{r_{\text{H},d}}{r_0} \left(\frac{M_{\text{edge}}}{2\pi M_d r_{\text{H},d}} \right)^{1/3}. \quad (39)$$

The disk edge is separated from the satellite by $\sim r_{\text{H},\text{eff}}$. Thus, $r_d \approx (1 - \eta r_{\text{H},\text{eff}}/r_d) r_s$, where η is a constant of

⁹ In the nomenclature of this paper, $r_{d,\text{edge}}$ should really be r_d . However, I will introduce this variable as I will fit for this and $r_{\text{H},\text{eff}}$.

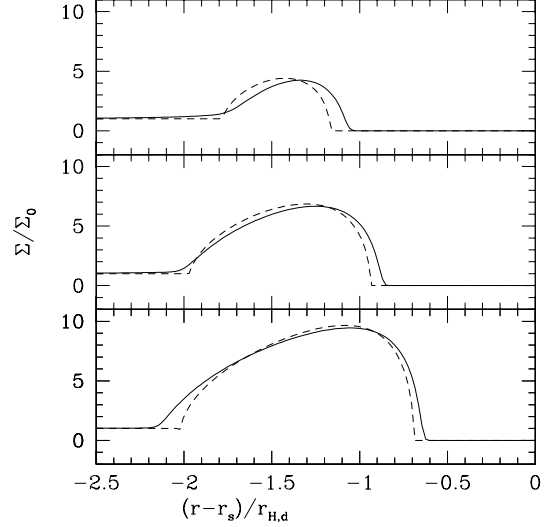


FIG. 6.— The surface density enhancement Σ/Σ_0 as a function of $(r - r_s)/r_{\text{H},d}$ for the approximate solution (dashed lines) and the numerical solution (solid lines) for a satellite disk system where $q' = 0.1$ for $\alpha' = 0.1$ and $\beta' = 1$. The snapshots are separated in $\Delta t = 0.5 t_{\text{df},0}$ increments and the corresponding position of the shepherding satellite (from top to bottom) is $r_s/r_{d,0} = 0.95, 0.75,$ and 0.65 .

order unity. Equating the time derivative of L (eq.[37]) and (2), I find

$$\frac{GM_s^2}{r_s} \sim \dot{L} = v_{\text{orb}} \left[M_s + M_{\text{edge}} \left(1 - \eta \frac{r_{\text{H},\text{eff}}}{r_d} \right) \right] v_{\text{shep}}, \quad (40)$$

where I ignore the time derivatives on M_{edge} . This gives

$$v_{\text{shep}} \sim v_{\text{orb}} \frac{M_s}{M_{\text{enc}}(r_s)} \frac{M_s}{M_s + M_{\text{edge}} (1 - \eta r_{\text{H},\text{eff}}/r_d)} \quad (41)$$

Despite its crudeness, this velocity estimator gives reasonably good agreement ($\lesssim 10\%$) when I select $\eta = 1$ and $\psi = 2$ via trial and error. I plot the comparison in Figure 5.

Equations (30), (32), (33), (34), and (41) constitute a complete analytic solution once the evolution of the disk can be modeled as kinematic wave, i.e., after the satellite sinks down a few $r_{\text{H},d}$. This approximate solution agrees well with the exact numerical solution as shown in Figure 6 for $q' = 0.1$. The agreement for $q' = 1$ and $q' = 0.01$ is not as good. For $q' = 1$, the assumption that $T_d \approx T_{\text{df}}$ breaks down and the agreement can be improved by estimating $T_d \approx T_{\text{df}}/(1 + q')$. For $q' = 0.01$, kinematic wave solutions are not established because the infall of the satellite is stopped.

Finally, from the estimate for v_{shep} given in equation (41) and Figure 5, I note v_{shep} is a factor of a few larger than $(M_s/M_d)v_{\text{df}}$, where v_{df} is taken at $r_{d,0}$. Hence I estimate the timescale for shepherding to be $t_{\text{shep}} \sim f(M_d/M_s)t_{\text{df}}$ or

$$t_{\text{shep}} \sim f \frac{M_d}{M_s} \frac{M_{\text{enc}}}{M_s} \frac{t_{\text{dyn}}}{\ln \Lambda}, \quad (42)$$

where $f < 1$ and $t_{\text{df}} \sim (M_{\text{enc}}/M_s)t_{\text{dyn}}/\ln \Lambda$.

4. THE FUELING OF CENTRAL STARBURSTS AND ACTIVE GALACTIC NUCLEI

As the satellite-disk system should continually shrink due to dynamical friction, it raises the interesting question of whether or not such a mechanism may be deliver gas into the nuclear regions of galaxies. The fueling of central starbursts and active galactic nuclei remains an open question. It is generally believed that the fueling of central starbursts and active galactic nuclei (AGNs) requires the delivery of gas from large radii to small radii (for a review see Shlosman, Begelman, & Frank 1990; hereafter SBF90). Gas transport is mediated at small radii (~ 1 pc) by a thin accretion disk. At much larger radii ($\gtrsim 0.1 - 1$ kpc), galactic bars can efficiently transport gas.

How is gas transported in the gap between $0.1 - 1$ kpc to ~ 1 pc? Galactic bars, while efficient at large scales, stop at the inner Lindblad resonance (ILR), which is at $\sim 0.1 - 1$ kpc.¹⁰ Thin accretion disks, which are sufficient at small scales, would become gravitationally unstable and would fragment to form stars outside of ~ 1 pc (Paczynski 1978; Kolykhalov & Sunyaev 1980; Shlosman & Begelman 1987; Goodman 2003; Thompson, Quataert & Murray 2005).

There are several possible modes by which this transport may be accomplished. First the gas is transported by large-scale *gaseous* gravitational instabilities, i.e., the “bars within bars” model (Shlosman, Frank, & Begelman 1989). Secondly, the gas may form a thick turbulent marginally stable accretion disk powered by star formation (Paczynski 1978; Kolykhalov & Sunyaev 1980; Shlosman & Begelman 1987; Goodman 2003) via radiation pressure (Goodman & Tan 2004; Thompson et al. 2005) or supernova (Wada & Norman 2002). Third, if the gas exist in the form of molecular clouds, collisions between them may lead to episodic feeding of the nuclear regions, i.e., the chaotic accretion scenario (Krolik & Begelman 1988; SBF90; Hopkins & Hernquist 2006; King & Pringle 2007; Nayakshin and King 2007). Finally, the fueling of these central regions by be one of brute force, where major or minor mergers drive gas from the disk of the galaxy to the nuclear region (Hernquist 1989; Bekki & Noguchi 1994; Mihos & Hernquist 1994; Hernquist & Mihos 1995)

In the “bars within bars” scenario, Shlosman, Frank, & Begelman (1989) argued that if a gravitationally unstable gas disk is sufficiently massive such that it fulfills the Ostriker-Peebles criterion (Ostriker & Peebles 1973), it forms a secondary gaseous bar which funnels gas inward on a dynamical time. Numerical simulations confirmed the viability of “bars within bars” (see for instance Friedli & Martinet 1993; Levine et al 2007). It demands a substantial mass in gas, $M_{\text{gas}} \sim M_{\text{enc}}$, where M_{enc} is the enclosed mass. While such large gas concentrations are observed (see for instance Jogee et al. 2005), delivered into the nuclear region by large scale bars, it is unclear if this mechanism drives the bulk of AGN fueling and quasar activity. Namely, the observed correlation between large-scale bars, which transports gas into the central region of galaxies, and Seyfert activity is statistically marginal (see the review by Ho 2008 and references

therein; see the review by Combes 2003 and references therein; but also see Laine et al 2002). In addition, there is no evidence that Seyferts have a higher fraction of nuclear bars (see Knapen 2004 and references therein).¹¹

On the other hand, if the disk is gravitationally unstable but lacks sufficient mass to fulfill the demands of “bars within bars”, the gas will fragment and form stars. The process of star formation may feed back on the disk to provide vertical support, maintaining marginal stability, i.e., $Q \sim 1$, where Q is the Toomre Q (see for instance Shlosman & Begelman 1989; Goodman 2003; Goodman & Tan 2004; Thompson et al. 2005). These thick marginally stable disks may have a sufficiently large scaleheight such that accretion via viscous processes is possible before all the gas is consumed.

Third, perhaps the gas exist primary in the form of molecular clouds. Collisions between these molecular clouds provides something akin to a viscosity (Krolik & Begelman 1988; SBF90). These clouds would then feed the nuclear region in a chaotic fashion (Hopkins & Hernquist 2006; King & Pringle 2007; Nayakshin and King 2007). Typically, the viscosity due to cloud-cloud collision appears to be insufficient for fueling the central regions from hundreds of parsecs. However, it may be necessary around the sphere of influence of the central black hole where large scale instabilities may not operate (SBF90; see §4.4)

Fourth, the fueling of central nuclear activity need not be due to gas in the ISM, but gas liberated from disrupted stars. Hills (1975) proposed that the tidal disruption of stars (Rees 1988) may be a means by which active galaxies may be fueled. These rates of tidal disruption are enhanced in mergers of galaxies (Roos 1981), which links the three phenomenon of merging galaxies, active galactic nuclei, and tidal disruption of stars. Alternatively, a pre-existing gas disk may capture stars plunging through it, subsequently disrupting these stars, which replenishes the disk. This gas may then viscously accrete, fueling the central engine (Miralda-Escudé & Kollmeier 2005).

Finally, mergers between galaxies may drive gas toward the nuclear regions of galaxies where they fuel nuclear activity (Hernquist 1989; Bekki & Noguchi 1994; Bekki 1995). This possibility may fuel ultraluminous infrared galaxies and quasar activity as modeled, for instance, by Springel et al. (2005) and Hopkins et al. (2005) and has significant observational support (see for instance Sanders et al 1988). However, active galactic nuclei (AGN) activity appears to be due to more quiescent phenomenon (Li et al 2006; Hopkins & Hernquist 2006). For instance, Li et al. (2006) explored the clustering properties of AGN in Data Release 4 of the Sloan Digital Sky Survey (SDSS) and concluded that interactions are unlikely to be the main culprit in the fueling of AGNs. Minor mergers are another possibility (see for instance Mihos & Hernquist 1994; Hernquist & Mihos 1995; Tanguchi & Wada 1996; Taniguchi 1997, 1999).

4.1. Fueling via Gas Shepherding

¹⁰ As pointed out by the referee, ILRs may or may not exist, depending on the nuclear mass concentration. However, these bars still become inefficient at small scales, i.e., typically 10% of the size of the bar (Shlosman, Frank, & Begelman 1989).

¹¹ As pointed out by the first referee, however, the nuclear bars may be very short lived and therefore, may be very difficult to observed.

Gas shepherding is another scenario by which gas is transported from hundreds of parsecs. The gas shepherding scenario, which I present is as follows: large scale bars drive gas toward the central regions of a galaxy where they collect in a nuclear ring, i.e. the gas transitions from X_1 to roughly circular X_2 orbits (Binney & Tremaine 1987) at a radii of a few hundred parsecs to 1-2 kiloparsecs (Buta & Combes 1996; Knapen 2004). This gaseous ring becomes gravitationally unstable and forms giant molecular clouds which in turn collapse to form star clusters in coplanar orbits (see for instance, Maoz et al. 2001; Jogee et al. 2002). If the star cluster formed is sufficiently massive, it may shepherd in the remnant gas in the gaseous ring from a few hundred parsecs into the center.

I first compare the timescale of shepherding and viscous processes. For an α viscosity, the viscous timescale is $t_{\text{visc}} \sim \alpha^{-1} (r/h)^2 t_{\text{dyn}}$ (Frank, King, & Raine 2002). For a marginally stable disk, i.e., $Q \sim 1$, $h/r \sim M_d/M_{\text{enc}}$. Therefore the ratio between the shepherding timescale, t_{shep} , and the viscous timescale, t_{visc} , is

$$\begin{aligned} \frac{t_{\text{shep}}}{t_{\text{visc}}} &\sim \frac{f\alpha}{\ln \Lambda} \frac{M_d}{M_{\text{enc}}} \left(\frac{M_d}{M_s}\right)^2, \\ &\sim 10^{-3} \left(\frac{\alpha}{0.1}\right) \left(\frac{f/\ln \Lambda}{0.1}\right) \left(\frac{M_d/M_s}{3}\right)^2 \\ &\quad \left(\frac{M_d/M_{\text{enc}}}{0.01}\right). \end{aligned} \quad (43)$$

These timescales become comparable to each other for thicker disks, i.e. $h/r \sim M_d/M_{\text{enc}} \sim 1$, or lower mass satellites, i.e., $M_d/M_s \sim 100$ or a combination of the two. Thus when shepherding operates, it dominates over viscous processes for low mass disk and large satellites. Therefore, for this scenario to work, the star cluster that is formed must be sufficiently massive compared to the mass of the gas disk. I would expect it to be at least 10% or greater in order for shepherding to be efficient based on equation (43) and on my calculations in §3.

If gas shepherding operates, what ultimately happens to this shepherded gas? First, if this gas is in a marginally stable disk, it may fragment into stars at the disk edge (see for instance Thompson et al. 2005; Levin 2007; Chang et al. 2007; Nayakshin, Cuadra, & Springel 2007; Van der Ven & Chang in preparation). Secondly, this gas may be shepherded into a radius where the shepherding satellite is tidally disrupted. I now discuss these two possibilities below.

4.2. Disk Fragmentation and Star Formation

Marginally stable disks with sufficiently rapid cooling ($t_{\text{cool}} < 3t_{\text{dyn}}$) will tend to fragment (Gammie 2001). In the galactic context this fragmentation will lead to star formation, which may feed back on the disk, maintaining marginal stability. This feedback may be due to momentum driving (Murray, Quataert, & Thompson 2005; Thompson et al. 2005), cosmic ray feedback (Socrates, Davis, & Ramirez-Ruiz 2008), or supernovae driven turbulence (Wada & Norman 2002). A surface density enhancement of a few to ten would enhance local star formation. I take the standard Kennicutt law (Kennicutt

1998) for the star formation rate to be

$$\dot{\Sigma}_* = \Sigma \Omega \eta, \quad (44)$$

where $\dot{\Sigma}_*$ is the star formation rate per unit area, Σ is the gas surface density, $\eta \sim 0.01$ is the empirically determined efficiency. Equation (44) suggests that the star formation rate would also be enhanced by the same factor as that of the surface density.

Equation (44) implies that the timescale for the gas to fragment into stars is

$$t_* \sim \frac{\Sigma}{\dot{\Sigma}_*} = \eta^{-1} t_{\text{dyn}}. \quad (45)$$

The ratio between the timescale for shepherding and the timescale for the gas to fragment into stars is

$$\begin{aligned} \frac{t_{\text{shep}}}{t_*} &\sim \eta \frac{f}{\ln \Lambda} \left(\frac{M_d}{M_s}\right)^2 \frac{M_{\text{enc}}}{M_d} \\ &\sim 1 \left(\frac{\eta}{0.01}\right) \left(\frac{f/\ln \Lambda}{0.1}\right) \left(\frac{M_d/M_s}{3}\right)^2 \\ &\quad \left(\frac{M_{\text{enc}}/M_d}{100}\right). \end{aligned} \quad (47)$$

Thus, sufficiently large satellites can shepherd a considerable fraction of the gas into the central regions before the gas completely fragments into stars. For typical numbers ($M_{\text{enc}} \sim 10^9 M_\odot$), this implies a satellite mass $\sim 10^6 M_\odot$.

For less massive satellites, the disk would completely fragment into stars. Thus, the evolution would likely be different. As the satellite continues to fall inward, it captures these newly-formed stars into mean-motion and secular resonances, which increases the star's eccentricity and inclination. Indeed, Yu, Lu, & Lin (2007) have suggested that this exact process may be responsible for the distribution of the young stars in the Galactic Center (GC). In this case, an intermediate-mass black hole (IMBH) or dark cluster falls into a disk of stars in the same orbital plane. The stellar disk is heated up as the stars are captured into the previously-mentioned resonance. Some of these stars are forced to migrate with the infalling IMBH, while others are forced into close encounters. Some of these stars that are subjected to these close encounters may be ejected out of the GC at large velocities, producing hypervelocity stars (HVSs) or hypervelocity binaries (HVBs) (Lu, Yu, & Lin 2007). Hence stars, whose semi-major axis is larger than the current radius of the infalling IMBH would be excited into a torus-like structure, while stars interior to the radius of the infalling IMBH would remain in a cold disk. Such a dynamical distribution may result from the effects of shepherding, but at much larger scales, i.e., ~ 100 pc rather than ~ 0.4 pc as in the case in the GC.

4.3. Destruction of the Shepherd

If this gas does not fragment into stars (which is the case for sufficiently massive satellites), gas shepherding may transport a substantial amount of gas from ~ 0.1 kpc to smaller radii. As long as the satellite remains coherent, there is no limit to how far gas may be shepherded. This requirement that the satellite be sufficiently massive ($\sim 10^6 M_\odot$) limits the number of possible systems that can serve as a shepherd.

A super star cluster (SSC) is one such candidate. SSCs range up to mass of $\sim 10^6 - 10^7 M_\odot$ with a radius of parsecs (see for instance McCrady & Graham 2007; Hagele et al. 2007) so they are sufficiently massive to transport gas before it completely fragments into stars. However, as they sink deeper into the bulge, tidal forces may disrupt them, stopping the shepherding process. The SSC is tidally disrupted when the enclosed background density $\rho_{\text{enc}} \propto r^{-2}$ is equal to their mean stellar density, $\rho_{\text{SSC}} \sim M_{\text{SSC}}/a_{\text{SSC}}^3$, where a_{SSC} is the radial size of the SSC. Plugging in a few example numbers, I find that $\rho_{\text{SSC}} \sim 10^6 (M_{\text{SSC}}/10^6 M_\odot) (a_{\text{SSC}}/1 \text{ pc})^{-3} M_\odot \text{ pc}^{-3}$. For typical numbers, i.e., $M_{\text{enc}} \sim 10^9 M_\odot$ at 100 pc, $\rho_{\text{enc}} \sim 10^7 (r/1 \text{ pc})^{-2} M_\odot \text{ pc}^{-3}$ so the radius where the satellite is disrupted is

$$r_{\text{tid}} \sim 12 \left(\frac{M_{\text{SSC}}}{5 \times 10^5 M_\odot} \right)^{-1/2} \left(\frac{a_{\text{SSC}}}{2 \text{ pc}} \right)^{3/2} \text{ pc}, \quad (48)$$

which would also be where the gas disk is shepherded down to. Note that I have ignored the effect of the SMBH, which begins to become important at such radii. The densities and density structures of these SSCs are not very well constrained. McCrady and Graham (2007) presents a very detailed study of the size and mass distribution of super star clusters in the nearby starbursting galaxy M82. The mean half power radius of these SSCs is 1.8 pc (McCrady and Graham 2007, their Figure 7), and there are quite a few clusters around $5 \times 10^5 M_\odot$. By equation (48), this gives a tidal disruption radius of about 10 pc. Lets consider two examples in more detail. One example is SSC L in M82 which has a virial mass of $\approx 4 \times 10^6 M_\odot$, a projected half-light radius of $\approx 1.5 \text{ pc}$, and a tidal disruption radius of $r_{\text{tid}} \approx 3 \text{ pc}$. Another example is SSC 11, which has a virial mass of $\approx 4 \times 10^5 M_\odot$, a projected half light radius of $\approx 1.1 \text{ pc}$, and a tidal disruption radius of $\approx 6 \text{ pc}$. In another study, Hagele et al (2007) observed five star forming regions of the circumnuclear ring of NGC 3351 and found star cluster masses between 1.8 – 8.9 M_\odot and radii of 1.7 – 4.9 pc. This would bracket tidal disruption radii between a few parsecs to 25 parsecs. Hubble space telescope studies by Maoz et al (1996) suggest that the star clusters formed in circumnuclear rings have sizes $< 5 \text{ pc}$. Hence, SSCs appears have sufficient mass and density to shepherd gas into ten to tens of parsecs.

The destruction of a SSC may not be the result of tidal processes, but instead to internal processes, i.e., stellar mass loss. Thus, SSCs may have a short lifetime in analogy with stellar clusters in our galaxy, i.e., open clusters and OB associations. For typical galactic clusters, they are disrupted because gas ejection from the formation of HII regions and supernova (Lada and Lada 2003). However, SSCs are thought to be the progenitors of globular clusters, whose lifetime is $\sim 10^{10}$ years, and thus their lifetime may be substantially longer. The vulnerability of SSCs to these internal processes strongly depend on their stellar initial mass functions, i.e., they must have a sufficient number of low mass stars (Meurer et al 1995). Top-heavy IMFs are vulnerable to the disruptive processes of stellar mass loss and other processes (Chernoff & Weinberg 1990). Young, dense stellar clusters, the closest local analogues to SSCs, show a significant population of

low mass stars. For instance, the $2 \times 10^4 M_\odot$ (Walborn et al 2002) stellar cluster, R136 in the Large Magellanic Cloud has a large population of low mass stars down to $0.1 M_\odot$ (Brandl et al 1996). In addition, McCrady et al. (2003) found SSC 9 was consistent with a normal IMF, though SSC 11 appeared to have a top heavy IMF.

Aside from SSCs, the nucleated remains of an accreted satellite galaxy may also be the shepherds that herds that gas into the central regions of the galaxy for sufficiently small mass ratios. For mass ratio between the mass of the satellite galaxy’s remnant and the *dynamical mass* is of order 10% or greater, long range tidal interactions may disrupt a central disk before the shepherding scenario outlined above can be set up and would be akin to the minor merger scenario studied previously (Hernquist 1989; Bekki & Noguchi 1994; Mihos & Hernquist 1994; Hernquist & Mihos 1995; Tanguchi & Wada 1996; Taniguchi 1997, 1999). Using the nucleated remains of satellite galaxies as shepherds is interesting, but a detailed study of this scenario is left to future work.

4.4. The Final Ten (or Tens of) Parsecs

As I argue in §4.3, SSCs can shepherd gas to within 10 to 10s of parsecs of the center. However, due to tidal disruption of the shepherds, gas shepherding is less effective at these small radii as a mechanism to drive gas further inward. A similar problem exists for the “bars within bars” scenario. Once gaseous bars funnel the gas within the gravitational sphere of influence of a black hole, it becomes increasingly difficult to have a sufficient amount of mass to form nested bars (SBF90 their Figure 2). As a result, another means of gas transport between ten to tens of parsecs must operate for the gas shepherding and “bars within bars” scenarios, i.e., the “10 parsec” problem. One possibility, outlined by SBF90, are cloud-cloud collisions. At the deposition radius, the gas becomes marginally self-gravitating and fragments into molecular clouds whose collisions with one another serves as a source of viscosity which drives material into the central regions. Typically, the viscosity scales like:

$$\alpha_{\text{cl-cl}} = \begin{cases} C & \text{for } C \ll 1 \\ C^{-1} & \text{for } C \gg 1 \end{cases}, \quad (49)$$

where C is the filling fraction of the clouds (see SBF90). It is unclear if this is more effective than magnetic (see the review by Balbus 2003) or gravitationally driven viscosities (Gammie 2001).

The effects of cloud-cloud collisions on the velocity dispersion of the clouds is not known. The internal structure, i.e., magnetic fields, will play a huge role in determining the efficiency of cloud-cloud collisional driven viscosity (see for instance Krolik & Begelman 1988). Another way by which this final “10 pc problem” can be solved is via a disk which is supported either by radiation pressure (Thompson et al. 2005), supernova driven turbulence (Wada & Norman 2002; Kawakatu & Wada 2008), or cosmic ray pressure (Socrates, Davis, & Ramirez-Ruiz 2008). The gas disk or ring which results from the deposition of gas at ten to tens of parsecs may form a marginally stable disk which is supported by star formation/supernova which can then viscously accrete. One-zone calculations by Thompson et al. (2005) suggest that a star formation rate of $\sim 1 M_\odot \text{ yr}^{-1}$ is sufficient to

support a marginally stable disk at ten to tens of parsecs (see Thompson et al. 2005, their Figure 5),¹² while also allows for a nontrivial accretion rate onto the central black hole. I note that the strengths of the “bars within bars” or gas shepherding scenarios and that of the starburst supported disk scenario are complementary to one another. Inside of tens of parsecs, modest star formation rates can support a radiation pressure supported disk rather than requiring $200 - 600 M_{\odot} \text{ yr}^{-1}$ star formation rates from 200 pcs inward (again see Thompson et al. 2005, their Figure 5). Recent observation of NGC 3227 by Davies et al. (2006) support this notion of star formation in a gas disk at small radii. However, the current star formation rate of $\sim 0.1 M_{\odot} \text{ yr}^{-1}$ appears to be insufficient to support the vertical scale of the disk. Other forms of pressure support, i.e., cosmic ray pressure (see Socrates, Davis, & Ramirez-Ruiz 2007 their appendix E), may be important in this context.

5. DISCUSSION AND CONCLUSIONS

I have calculated the action of an infalling satellite on a coplanar gaseous disk. The satellite falls inward because of dynamical friction and couples to the gaseous disk via disk tides. Due to the unrelenting loss of angular momentum, the satellite-disk system shrinks in radius. Thus, gas is transported from larger radii to smaller radii. I calculate the structure of the evolving disk as a function of radius, both numerically and analytically and show a significant density enhancement at the disk edge. This density enhancement is due to the transport of gas initially at larger radii to a ring that is $r_{\text{H,d}}$ thick radially.

The fate of this shepherded gas is not known. I presented two possible outcomes: 1. the gas will fragment and form stars or 2. the gas is shepherded into the nuclear region. In the latter case, I suggest that the gas shepherding scenario, which I have presented may be one means by which the “100 parsec” problem may be resolved. For this to occur, gas must be shepherded sufficiently rapidly such that the gas is not completely consumed in star formation, which requires a sufficiently massive satellite ($\sim 10^6 M_{\odot}$). I argue that such massive satellites exist on the form of SSCs.

In the model presented, the physics of star formation in a disk environment has not been fully addressed. Observationally, galactic star-forming disks appear to be marginally unstable to fragmentation, i.e., $Q \sim 1$ (Thompson et al 2005) and their star formation rate follows the Kennicutt law (Kennicutt 1998). These two points suggests that some sort of feedback is responsible for maintaining this careful balance between fragmentation and heating. How this feedback operates is not well understood. As discussed previously, various models have invoked radiation pressure (Thompson et al. 2005), supernova feedback (Wada & Norman 2002), and cosmic ray pressure (Socrates et al. 2008) from star formation. Alternatively, the turbulent pressure support may result from gravitational instability, i.e., gravitoturbulence (Gammie 2001). It is unclear that in the presence of gas shepherding if this equilibrium can be maintained at the edge of the disk where the surface density is enhanced. If it does not, this edge is likely to fragment completely

into stars on a few dynamical times. It is also unclear if the Kennicutt law would continue to hold at the disk edge. Additional insights from future research on self-gravitating star-forming galactic disks will be needed to help formulate a more self-consistent calculation of the gas shepherding scenario, which will be needed to fully address the fate of the shepherded gas.

Assuming that the gas is not fully consumed in star formation, it would be shepherded down to 10 to 10s of parsecs (see §4.4). At that radii cloud-cloud collisions (Krolik & Begelman 1988; SBF90) or a starburst supported disk (Thompson et al. 2005) would allow the material to be viscously accreted.

The initial satellite inclination and/or eccentricity is likely to significantly affect gas shepherding. In this paper, I have studied a special case where the orbit of the satellite is in the plane of the disk and approximately circular for simplicity. An eccentric satellite would have its eccentricity damped via the excitation of spiral density waves. If the eccentricity is below $r_{\text{H,d}}/r_{\text{d}}$, i.e., the satellite stays within one “Hill radius” of the disk of its outer edge, then the shepherding calculation presented should be a reasonable estimate of the shepherding timescales and velocities.

Compared to a coplanar satellite, an inclined satellite would couple less well to the gaseous disk. For a sufficiently large inclination, the gas disk and satellite would be effectively decoupled. However, its inclination could be sufficiently rapidly damped via induced bending waves in the gas disk in addition to spiral density waves (see for instance Ostriker 1994; Terquem 1998). Once its inclination is damped below the critical value, where the disk and satellite become well coupled, the shepherding scenario presented in this paper would likely follow. I would expect this critical inclination to be of order $\sin i = r_{\text{H,d}}/r_{\text{d}}$, i.e., the satellite stays within of order a “Hill radius” of the disk above and below it.

Extending the present calculation to satellites of modest inclination would be fruitful and would allow a study of using the nucleated cores from minor mergers as shepherding satellites (see §4.3). As discussed in §4, minor mergers may drive nuclear activity. The initial inclination of minor mergers is arbitrary, but their inclination is damped as they interact with the *large scale* stellar and gaseous disk. As a result, they may approach the shepherding scenario presented in this paper. Such a study is a subject for future work.

In addition, dynamical friction would also act on the satellite-induced spiral density waves. Dynamical friction of the extended mass perturbation, i.e., the satellite-induced spiral density waves, may enhance the transfer of angular momentum between the gas disk and background stars (Tremaine & Weinberg 1984). A study of these effects, while fruitful, is beyond the scope of this work.

The physics of gas shepherding is also important in other areas as well. For instance, it may shape radial distribution of star clusters in nuclear gas rings. In some of these nuclear ring systems, the location of the star clusters is exterior to the gas ring from which they are presumably formed. For instance, NGC 4314 clearly show the star clusters exterior to the gas (Benedict et al. 2002). Martini et al. (2003) found that the eight galaxies with strong bars all have star formation exterior

¹² I note, however, that they presume some sort of global torque via spiral arms or the like in their calculations.

to the dust ring in their sample of 123 galaxies. How gas shepherding drives this morphology is the subject of a forthcoming work. (Van der Ven & Chang, in preparation).

I thank N. Murray for his early encouragement and useful discussions. I thank A. Socrates for his advice and continuing encouragement. I thank R. Levine and A. Kratsov for making an early copy of their manuscript available. I thank E. Quataert for useful discussions and a careful reading of this manuscript. I also thank G.

Van der Ven and E. Chiang for useful discussions. I thank M. Jones for a careful reading of this manuscript. I thank the anonymous referees for very useful comments which improved the presentation of this paper. I also thank the Kavli Institute for Theoretical Physics and the Max-Planck Institute for Astrophysics for their hospitality during the initial and final stages of this project, respectively. I gratefully acknowledge the support of the Miller Institute for Basic Research. This research was supported in part by the National Science Foundation under Grant No. PHY05-51164

APPENDIX

CALCULATION OF σ_{MAX}

I now discuss the calculation of σ_{max} and hence derive the constant of integration C . I first plug equation (30) into equation (27) to find

$$x_{\text{d},0}^{-1} \frac{\partial x_{\text{s}}}{\partial t'} = 2\beta' \left(\frac{x_{\text{s}}}{x_{\text{d},0}} \right)^3 \int \sqrt{C + \frac{q'}{\alpha' q_{\text{d}}^{1/3}} \left(-\frac{2}{3} v_{\text{shep}} x + \frac{2\beta'}{9} \left(\frac{x_{\text{s}}}{x_{\text{d},0}} \right)^2 \frac{q'}{q_{\text{d}}^{2/3}} \left(\frac{1}{x^3} \right) \right)} \frac{dx}{x^4} - \frac{x_{\text{d},0}}{x_{\text{s}}}. \quad (\text{A1})$$

I make the approximation that the torque due to the satellite-disk interaction and the torque from dynamical friction nearly cancel each other out, i.e., $x_{\text{d},0}^{-1} \partial x_{\text{s}} / \partial t' \ll 1$. Hence I find,

$$2\beta' \int \sqrt{C + \frac{q'}{\alpha' q_{\text{d}}^{1/3}} \left(-\frac{2}{3} v_{\text{shep}} x + \frac{2\beta'}{9} \left(\frac{x_{\text{s}}}{x_{\text{d},0}} \right)^2 \frac{q'}{q_{\text{d}}^{2/3}} \left(\frac{1}{x^3} \right) \right)} \frac{dx}{x^4} = \left(\frac{x_{\text{d},0}}{x_{\text{s}}} \right)^4. \quad (\text{A2})$$

It is helpful to break the integral in equation (A2) into two parts. I rewrite the integral, I , as

$$I \equiv \int \rightarrow \int_{-\infty}^{x_{\text{peak}}} + \int_{x_{\text{peak}}}^{x_{\text{max}}}, \quad (\text{A3})$$

where $x_{\text{max}} < x_{\text{s}}$ is defined as where $\sigma_{\text{w}}(x > x_{\text{max}}) = 0$, i.e., the disk is cutoff by disk tides above this radius, and consider each integral in turn. The first integral, I_1 , is

$$I_1 \equiv \int_{-\infty}^{x_{\text{peak}}} \sqrt{C + \frac{q'}{\alpha' q_{\text{d}}^{1/3}} \left(-\frac{2}{3} v_{\text{shep}} x + \frac{2\beta'}{9} \left(\frac{x_{\text{s}}}{x_{\text{d},0}} \right)^2 \frac{q'}{q_{\text{d}}^{2/3}} \left(\frac{1}{x^3} \right) \right)} \frac{dx}{x^4}. \quad (\text{A4})$$

At x_{peak} , $\sigma_{\text{w}} = \sigma_{\text{max}}$ and it declines as x becomes more negative, i.e., away from the satellite, because of the $v_{\text{shep}} x$ term in the square root. However, the torque density declines even faster, so I may approximate $\sigma_{\text{w}} = \sigma_{\text{max}}$ for the purposes of this integral, i.e.,

$$I_1 \approx \int_{-\infty}^{x_{\text{peak}}} \frac{\sigma_{\text{max}}}{x^4} dx = \frac{1}{3} \frac{\sigma_{\text{max}}}{x_{\text{peak}}^3}. \quad (\text{A5})$$

The second integral, I_2 , is

$$I_2 \equiv \int_{x_{\text{peak}}}^{x_{\text{max}}} \sqrt{C + \frac{q'}{\alpha' q_{\text{d}}^{1/3}} \left(-\frac{2}{3} v_{\text{shep}} x + \frac{2\beta'}{9} \left(\frac{x_{\text{s}}}{x_{\text{d},0}} \right)^2 \frac{q'}{q_{\text{d}}^{2/3}} \left(\frac{1}{x^3} \right) \right)} \frac{dx}{x^4}. \quad (\text{A6})$$

Here, the disk torque increases as x approaches x_{max} , but σ_{w} declines due to the x^{-3} term in the square root. As the linear term $v_{\text{shep}} x$ is overwhelmed by x^{-3} as x approaches smaller *absolute* values i.e. $x \rightarrow x_{\text{max}}$, I ignore the linear term and approximate this integral by

$$I_2 \approx \int_{x_{\text{peak}}}^{x_{\text{max}}} \sqrt{C + \frac{q'^2}{\alpha' q_{\text{d}}} \frac{2\beta'}{9} \left(\frac{x_{\text{s}}}{x_{\text{d},0}} \right)^2 \left(\frac{1}{x^3} \right)} \frac{dx}{x^4}. \quad (\text{A7})$$

Changing variables to

$$y = C + \frac{q'^2}{\alpha' q_{\text{d}}} \frac{2\beta'}{9} \left(\frac{x_{\text{s}}}{x_{\text{d},0}} \right)^2 \left(\frac{1}{x^3} \right) \quad (\text{A8})$$

$$dy = -\frac{2\beta'}{3} \frac{q'^2}{\alpha'q_d} \left(\frac{x_s}{x_{d,0}}\right)^2 \frac{1}{x^4} dx, \quad (\text{A9})$$

and performing the integral, I find

$$I_2 \approx \beta'^{-1} \left(\frac{x_{d,0}}{x_s}\right)^2 \frac{\alpha'q_d}{q'^2} \left[\left(C + \frac{q'}{\alpha'q_d^{1/3}} \left(-\frac{2}{3} v_{\text{shep}} x + \frac{2\beta'}{9} \left(\frac{x_s}{x_{d,0}}\right)^2 \frac{q'}{q_d^{2/3}} \left(\frac{1}{x^3}\right) \right) \right) \right]^{3/2} \Bigg|_{x_{\text{max}}}^{x_{\text{peak}}}. \quad (\text{A10})$$

At x_{peak} the term in brackets, which I identify as my approximation for σ_w , is σ_{max}^3 , while at x_{max} , the term in brackets is 0. Thus I find

$$I_2 = \beta'^{-1} \left(\frac{x_{d,0}}{x_s}\right)^2 \frac{\alpha'q_d}{q'^2} \sigma_{\text{max}}^3 \quad (\text{A11})$$

Hence equation (A3) becomes

$$I = I_1 + I_2 \approx \frac{1}{3} \frac{\sigma_{\text{max}}}{x_{\text{peak}}^3} + \beta'^{-1} \left(\frac{x_{d,0}}{x_s}\right)^2 \frac{\alpha'q_d}{q'^2} \sigma_{\text{max}}^3. \quad (\text{A12})$$

Plugging this result into equation (A2) gives a cubic equation for σ_{max}

$$\frac{2\beta'}{3} \frac{\sigma_{\text{max}}}{x_{\text{peak}}^3} + 2 \left(\frac{x_{d,0}}{x_s}\right)^2 \frac{\alpha'q_d}{q'^2} \sigma_{\text{max}}^3 - \left(\frac{x_{d,0}}{x_s}\right)^4 = 0, \quad (\text{A13})$$

which I may solve numerically.

REFERENCES

- Artymowicz, P. 1993, *ApJ*, 419, 166
 Bath, G. T. & Pringle, J. E. 1981, *MNRAS*, 194, 967
 Bekki, K., & Noguchi, M. 1994, *A&A*, 290, 7
 Bekki, K. 1995, *MNRAS*, 276, 9
 Benedict, G. F., Howell, D. A., Jørgensen, I., Kenney, J. D. P., & Smith, B. J. 2002, *AJ*, 123, 1411
 Binney, J. & Tremaine, S. 1987, “Galactic Dynamics”, (Princeton University Press: Princeton)
 Brandl, B., Sams, B. J., Bertoldi, F., Eckart, A., Genzel, R., Drapatz, S., Hofmann, R., Loewe, M., & Quirrenbach, A. 1996, *ApJ*, 466, 254
 Buta, R., & Combes, F. 1996, *Fundamentals of Cosmic Physics*, 17, 95
 Chandrasekhar, S. 1943, *ApJ*, 97, 251
 Chang, P., Murray-Clay, R., Chiang, E., & Quataert, E. 2007, *ApJ*, 668, 236
 Chernoff, D. F. & Weinberg, M. D. 1990, *ApJ*, 351, 121
 Combes, F. 2003, SF2A-2003: Semaine de l’Astrophysique Française, meeting held in Bordeaux, France, June 16-20, 2003. Eds.: F. Combes, D. Barret, T. Contini, and L. Pagani., 243
 Davies, R. I., et al. 2006, *ApJ*, 646, 754
 Frank, J., King, A., & Raine, D. 2002, “Accretion Power in Astrophysics”, (Cambridge University Press: Cambridge)
 Friedli, D., & Martinet, L. 1993, *A&A*, 277, 27
 Gammie, C. 2001, *ApJ*, 553, 174
 Goldreich, P. & Tremaine, S. 1978, *Icarus*, 34, 240
 Goldreich, P. & Tremaine, S. 1980, *ApJ*, 241, 425
 Goldreich, P. & Tremaine, S. 1982, *ARA&A*, 20, 249
 Goodman, J. 2003, *MNRAS*, 339, 937
 Goodman, J. & Tan, J. C. 2004, *ApJ*, 608, 108
 Hägele, G. F., Díaz, Á. I., Cardaci, M. V., Terlevich, E., & Terlevich, R. 2007, *MNRAS*, 378, 163
 Hernquist, L. 1989, *Nature*, 340, 687
 Hernquist, L. & Mihos, J. C. 1995, *ApJ*, 448, 41
 Hills, J. G. 1975, *Nature*, 254, 295
 Ho, L. C. 2008, to appear in *ARA&A*, arXiv:0803.2268
 Hopkins, P. F. & Hernquist, L. 2006, *ApJS*, 166, 1
 Hopkins, P. F., Hernquist, L., Cox, T. J., Di Matteo, T., Robertson, B., & Springel, V. 2006, *ApJS*, 163, 1
 Hourigan, K. & Ward, W. R. 1984, *Icarus*, 60, 29
 Jøgee, S., Scoville, N., & Kenney, J. D. P. 2005, *ApJ*, 630, 837
 Kawakatu, N., & Wada, K. 2008, to appear in *ApJ*, arXiv:0803.2271
 Kennicutt, R. C., Jr. 1998, *ApJ*, 498, 541
 King, A. R., & Pringle, J. E. 2007, *MNRAS*, 377, L2
 Knapen, J. H. 2004, in Penetrating bars through masks of cosmic dust : the Hubble tuning fork strikes a new note, Ed. D. L. Block, I. Puerari, K. C. Freeman, R. Groess, and E. K. Block (Dordrecht: Kluwer)
 Kolykhalov, P. I. & Sunyaev, R. A. 1980, *Sov. Ast.*, 6, 35
 Krolik, J. H., & Begelman, M. C. 1988, *ApJ*, 329, 702
 Lada, C. J. & Lada, E. A. 2003, *ARA&A*, 41, 57
 Laine, S., Shlosman, I., Knapen, J. H., & Peletier, R. F. 2002, *ApJ*, 567, 97
 Levin, Y. 2007, *MNRAS*, 374, 515
 Levine, R., Gnedin, N. Y., Hamilton, A. J. S., & Kratsov, A. V. 2007, submitted to *ApJ*
 Li, C., Kauffmann, G., Wang, L., White, S. D. M., Heckman, T. M.; Jing, Y. P. 2006, *MNRAS*, 373, 457
 Lin, D. N. C. & Papaloizou, J. C. B. 1979a, *MNRAS*, 186, 799
 Lin, D. N. C. & Papaloizou, J. C. B. 1979b, *MNRAS*, 188, 191
 Lin, D. N. C. & Papaloizou, J. C. B. 1986, *ApJ*, 307, 395
 Lu, Y., Yu, Q., & Lin, D. N. C. 2007, *ApJ*, 666, L89
 Martini, P., Regan, M. W., Mulchaey, J. S., & Pogge, R. W. 2003, *ApJS*, 146, 353
 Maoz, D., Barth, A. J., Sternberg, A., Filippenko, A. V., Ho, L. C., Macchetto, F. D., Rix, H.-W., & Schneider, D. P. 1996, *AJ*, 111, 2248
 Maoz, D., Barth, A. J., Ho, L. C., Sternberg, A., & Filippenko, A. V. 2001, *AJ*, 121, 3048
 McCrady, N., Gilbert, A. M., & Graham, J. R. 2003, *ApJ*, 596, 240
 McCrady, N. & Graham, J. R. 2007, *ApJ*, 663, 844
 Meurer, G. R., Heckman, T. M., Leitherer, C., Kinney, A., Robert, C., & Garnett, D. R. 1995, *AJ*, 110, 2665
 Mihos, J. C. & Hernquist, L. 1994, *ApJ*, 425, L13
 Miralda-Escudé, J., & Kollmeier, J. A. 2005, *ApJ*, 619, 30
 Murray, N., Quataert, E., & Thompson, T. A. 2005, *ApJ*, 618, 569
 Nayakshin, S. & King, A. 2007, submitted to *MNRAS*, arXiv:0705.1686
 Nayakshin, S., Cuadra, J., & Springel, V. 2007, *MNRAS*, 379, 21
 Ostriker, E. C. 1994, *ApJ*, 424, 292
 Ostriker, J. P. & Peebles, P. J. E. 1973, *ApJ*, 186, 467
 Paczynski, B. 1978, *Acta Astron.*, 28, 91
 Papaloizou, J. C. B. & Lin, D. N. C. 1995, *ARA&A*, 33, 505
 Press, W. H., Teukolsky, S. A., Vetterling, W. T., & Flannery, B. P. 1992, “Numerical recipes in FORTRAN. The art of scientific computing” (Cambridge University Press: Cambridge)
 Rafikov, R. R. 2002, *ApJ*, 569, 997
 Rees, M. J. 1988, *Nature*, 333, 523
 Roos, N. 1981, *A&A*, 104, 218

- Sanders, D. B., Soifer, B. T., Elias, J. H., Madore, B. F., Matthews, K., Neugebauer, G., & Scoville, N. Z. 1988, *ApJ*, 325, 74
- Shakura, N. I., & Syunyaev, R. A. 1973, *A&A*, 24, 337
- Shlosman, I. & Begelman, M. C. 1987, *Nature*, 329, 810
- Shlosman, I., & Begelman, M. C. 1989, *ApJ*, 341, 685
- Shlosman, I., Begelman, M. C., & Frank, J. 1990, *Nature*, 345, 679 (SBF90)
- Shlosman, I., Frank, J., & Begelman, M. C. 1989, *Nature*, 338, 45
- Socrates, A., Davis, S. W., Ramirez-Ruiz, E. 2006, submitted to *ApJ*, astro-ph/0609796
- Springel, V., Di Matteo, T., & Hernquist, L. 2005, *MNRAS*, 361, 776
- Taniguchi, Y. 1997, *ApJ*, 487, L17
- Taniguchi, Y. 1999, *ApJ*, 524, 65
- Taniguchi, Y. & Wada, K. 1996, *ApJ*, 469, 581
- Terquem, C. E. J. M. L. J. 1998, *ApJ*, 509, 819
- Thompson, T. A., Quataert, E., & Murray, N. 2005, *ApJ*, 630, 167
- Toomre, A. 1964, *ApJ*, 139, 1217
- Tremaine, S. & Weinberg, M. D. 1984, *MNRAS*, 209, 729
- Wada, K., & Norman, C. A. 2002, *ApJ*, 566, L21
- Walborn, N. R., Maz-Apellniz, J., & Barb, R. H. 2002, *AJ*, 124, 1601
- Ward, W. R. & Hourigan, K. 1989, *ApJ*, 347, 490
- Ward, W. R. 1997, *Icarus*, 126, 261
- Yu, Q., Lu, Y., & Lin, D. N. C. 2007, *ApJ*, 666, 919